The Manufacturing Engineering Society International Conference, MESIC 2015

Morphology and mechanical characterization of ABS foamed by microcellular injection molding

J. Gómez-Monterde[a,b,]*, M. Schulte[b], S. Ilijevic[b], J. Hain[c], D. Arencón[a],
M. Sánchez-Soto[a], M. Ll. Maspoch[a]

[a]*Centre Català del Plàstic, Universitat Politècnica de Catalunya-BarcelonaTech (ETSEIB-ETSEIAT), Carrer Colom 114, Terrassa 08222, Spain.*
[b]*Centro Técnico de SEAT SA, Autovía A-2, km 585. Apartado de correos 91, Martorell 08760, Spain.*
[c]*Volkswagen AG, Wolfsburg D-38436, Germany.*

Abstract

In the present work ABS was used to inject cylindrical test bars, obtaining solid and foamed specimens. By varying the gas content, two levels of weight reduction were achieved. Morphology analysis revealed the presence of solid skin-foamed core structure in foamed samples. SEM micrographs showed a nucleus zone having bigger cells and irregular cell distribution, surrounded by a microcellular area with finer cell structure. Foamed bars with 10% and 17% of weight reduction presented similar values of cell size, cell density and solid skin thickness. On the other hand, results provided by simulation software were consistent with the experimental analysis. Mechanical properties were determined through tensile tests. Tensile strength and elastic modulus gradually decreased with decreasing apparent density. Experimental results were related to relative density and morphology parameters, and prediction models were employed to compare the estimated values to the experimental data.

Keywords: Microcellular injection molding; MuCell®; polymer foam; ABS.

1. Introduction

Climate change is one of the most important challenges facing the whole planet. Around 17% of greenhouse gas emissions are derived from the transport sector [1]. Thus, automotive industry focuses its efforts on decreasing CO_2

* Corresponding author. Tel.: +34-93-708-6353; fax: +34-93-784-18-27.
  E-mail address: javier.gomez@upc.edu

emissions and providing more sustainable road transportation. In this regard, replacing conventional materials with lighter alternatives arises as an appropriate strategy to reduce fuel consumption and carbon footprint [2].

Foaming technologies, such as the microcellular injection molding *MuCell®* process (*Trexel Inc.*), can enable car manufacturers to decrease weight in plastic components. By reducing the amount of material and cycle time, as well as processing temperatures and clamping force, automotive parts can be produced with a lower impact on the environment [3]. The influence of the processing parameters on cell structure and mechanical properties has been investigated in a wide range of plastics, such as PP, PC, PS, PA6, PLA, LDPE and PET, and reinforced polymers with nanoclay, talc particles or glass fibers.

In this study, Acrilonitrile-Butadiene-Styrene (ABS) was used as polymer matrix for foaming. Being an amorphous material, ABS absorbs more gas than crystalline polymers [4], mainly CO_2, although a higher diffusion of N_2 in ABS and a reduction in the glass transition temperature due to the gas content have been reported [5]. Many investigations have been made on ABS foamed by batch processes [6]. It has been concluded that the butadiene rubber in ABS behaves as foaming nucleus [7], improving the cell nucleation. Dong *et al.* [8] described the cell forming mechanisms of ABS during injection molding, and an improvement of the cell structure was obtained combining chemical and physical nucleating agents [9].

This work aims to provide the morphology characterization of ABS foams obtained by injection molding, as well as to analyze the effect of gas content and density reduction on the mechanical behavior.

Experimental setup

Material

A commercial grade of ABS (*Magnum™ 8434*), supplied by *Styron Netherlands B.V.*, was selected for this study. The material has a density of 1.05 g/cm^3 (ISO 1183/B) and a melt flow index of 13 g/ 10 min (ISO 1133), and it is commonly used in automotive interior trims.

Injection molding

Prior to the injection experiments, ABS was dried at 80 ºC for 4 hours. A four-cavity mold was employed to produce cylindrical bars of 300 mm in length and diameters of 4, 5 and 8 mm (Fig. 1) in a *Victory 110* injection molding machine (*Engel GmbH*), equipped with *MuCell®* supercritical fluid (SCF) supply system. The mold temperature was kept at 60ºC, and a constant melt temperature profile was used: 160-220-230-245-250ºC, from hopper to nozzle. Injection speed of solid bars was 70 cm^3/s, whereas it was 100 cm^3/s in case of foamed specimens. The selected shot volume was 85, 71 and 68 cm^3, corresponding to solid and foamed bars with 10% and 17% of weight reduction, respectively. N_2 was used as physical blowing agent, and the gas content of the two groups of foamed specimens was 0.6% and 0.93%. Cooling time was 30 seconds for all samples.
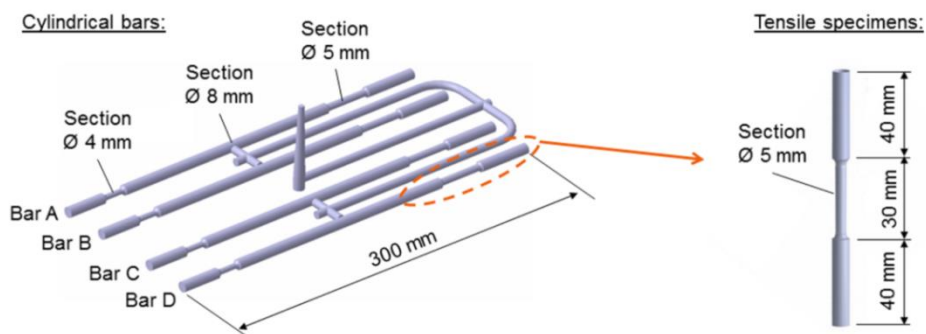

Fig. 1. Scheme of cylindrical bars and tensile test specimens.

Morphology and mechanical characterization

The apparent density was obtained by measuring weight and volume of 15 bars out of every mold cavity (A-D, Fig. 1). Morphology of foamed bars was analyzed in sections of 5, 8 and 4 mm in diameter, as shown in Fig. 1. Analysis surfaces were obtained by cryogenic fracture. Scanning Electron Microscopy (SEM) pictures were taken with a *JEOL JSM-560* microscope. Quantitative parameters such as cell size, cell density, skin thickness or foamed area were determined using *Igor Pro®* (*Wavemetrics Inc.*) and *Matlab®* (*The MathWorks Inc.*) software. Cell density (*N*) is referred as the number of cells per volume (cells/cm^3), and it is calculated as follows:

$$N = \left(\frac{n}{A}\right)^{\frac{3}{2}}\left(\frac{\rho_s}{\rho_f}\right)$$

(1)

Where *n* is the number of cells in the micrograph, *A* is the analyzed area (cm^2), and ρ_s and ρ_f are the density of solid and foamed material, respectively. *Moldex 3D®* software (*CoreTech System Co.*) was employed to simulate the injection molding process of the cylindrical bars and to compare the results to the ones obtained by experimental analysis.

Mechanical properties were determined using tensile tests. A minimum of 5 specimens with a diameter of 5 mm and a length of 110 mm were extracted from each bar and injection condition (Fig. 1). Tests were carried out on a universal testing machine *Zwick/Roell Amsler HC25/2008* (*Zwick GmbH & Co. KG*), at a crosshead speed of 50 mm/min and room temperature.

Results

Apparent density

During foaming, a lack of filling in cavity B was observed. Therefore, the bars of this cavity were not included in the experimental analysis. Table 1 shows the apparent density of bars A, C and D, injected in solid and foamed conditions.

Table 1. Apparent density of cylindrical bars.

Condition	Bar A	Bar C	Bar D
	ρ_A (g/cm^3)	ρ_C (g/cm^3)	ρ_D (g/cm^3)
Solid	0.977 ± 0.005	0.979 ± 0.004	0.979 ± 0.004
Foamed 1 (10% weight reduction)	0.900 ± 0.014	0.857 ± 0.015	0.905 ± 0.028
Foamed 2 (17% weight reduction)	0.820 ± 0.027	0.771 ± 0.012	0.836 ± 0.013

Solid bars presented the same density in the different cavities, with a slight standard deviation. However, considering the foamed samples, the outer bars were 6% denser than bar C in case of 10% of weight reduction, and 9% denser when the weight was decreased by 17%. Despite the symmetrical position of the cavities inside the mold, cooling of inner parts was different than cooling of outer bars. This is also the reason of the lack of filling in bar B. As obtained by means of injection process simulation with *Moldex 3D®* software, melt front time for bar A was longer than for bar B (Fig. 2). When solid samples were injected, all cavities were equally filled due to the holding pressure. But during foaming, the holding step was not employed and less amount of material was introduced in the mold cavity. Thereby, inner bars solidified faster, which gave rise to a lower packing of material and lighter or even not fully filled bars.
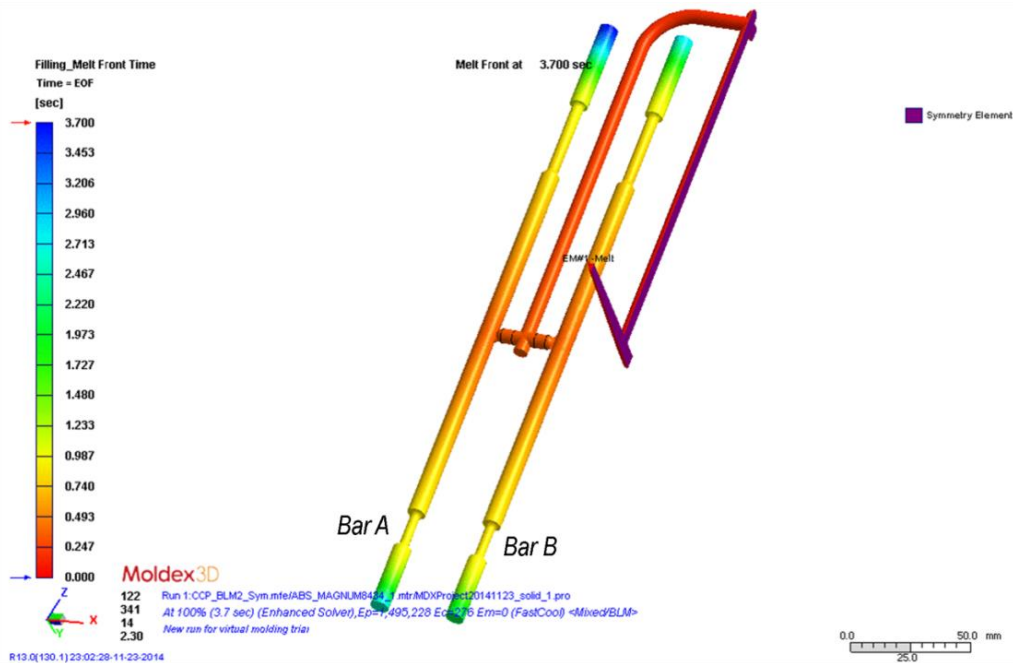
Fig. 2. Melt front time in cylindrical bars simulated with *Moldex 3D*® software.

Morphology

Fig. 3 and 5 show SEM micrographs taken in sections with a diameter of 5 and 8 mm for both groups of foamed bars. A typical solid skin-foamed core structure can be observed. Cells are distorted according to the circular section, and become higher as they are closer to the center. Due to the broad range of cell size, it seemed appropriate to divide the foamed core into two different areas [10]. The heat concentration and slower cooling rate in the middle section result in lower viscosity of the melt polymer, higher bubble growth and coalescence, which turn out bigger cells and irregular cell distribution in the nucleus. Between the skin layer and this nucleus, there is a microcellular zone with a more homogenous cell structure.

Cell size and cell density in the foamed nucleus and in the microcellular zone was determined, as well as in the overall foamed area. The analysis of cell distribution in sections with a diameter of 5 and 8 mm are shown in Fig. 4 and 6. Cell size varied from 6 to 200 μm in sections of 5 and 4 mm in diameter, but despite this wide range, around 95% of cells in the microcellular zone of both foaming conditions were smaller than 40 μm, with a central value located in 20 μm. The cell size in the nucleus was slightly more dispersed, but 95% of cells were smaller than 130 μm in case of 10% of weight reduction, and smaller than 70 μm in the second foaming level. In the middle section of the bar, with a thickness of 8 mm, the cell size reached a maximum value of 400 μm, with a more irregular cell distribution.

Cell density is kept in an order of magnitude of 10^6 cells/cm^3 in sections of 4 and 5 mm in diameter, and 10^4-10^5 cells/cm^3 in Ø=8 mm sections. A slight increase in cell density with the weight reduction ratio is observed in Fig. 7. That is, the introduction of a larger amount of gas increases the cell nucleation. The injected gas is, therefore, distributed into a higher number of smaller cells with more uniform size [11]. The morphology analyzed in the cross-section of 8 mm in diameter showed a broader cell size range (up to 400 μm) and an irregular distribution, as has been already commented. The high temperature in this section enables higher cell growth and expansion, as well as bubble coalescence. Shrinkage of the part during cooling could also contribute to higher cell sizes. As a result, a cell structure with bigger, non-uniform cells and lower cell densities is formed. For this reason, physical injection molding foaming processes are recommended to parts thinner than 4 mm [12].
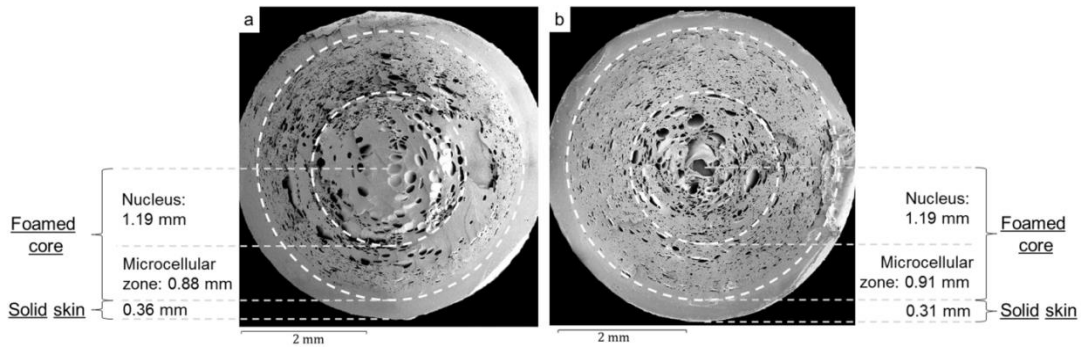
Fig. 3. SEM micrographs of Ø = 5 mm section and morphology areas of bar A with (a) 10% of weight reduction; (b) 17% of weight reduction.
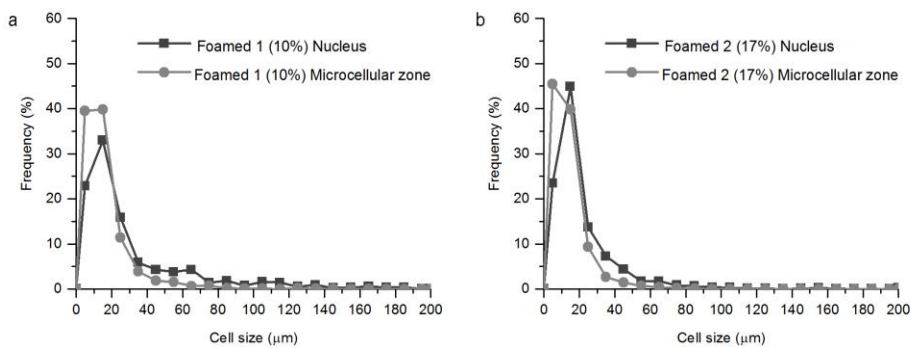

Fig. 4. Frequency cell size distribution in Ø = 5 mm section of bar A with (a) 10% of weight reduction; (b) 17% of weight reduction.

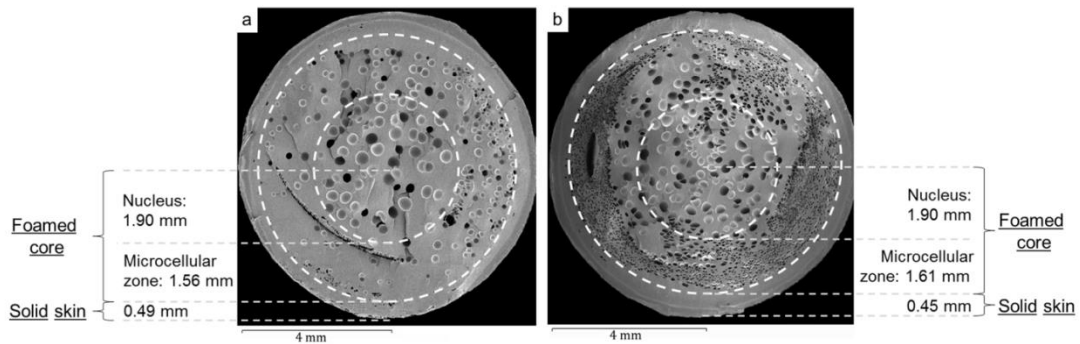Fig. 5. SEM micrographs of Ø = 8 mm section and morphology areas of bar A with (a) 10% of weight reduction; (b) 17% of weight reduction.

Simulation of injection process by means of *Moldex 3D®* software provided an average cell size of 40 µm in sections of 5 and 4 mm in diameter, and a cell density of $1.8 \cdot 10^6$ cells/cm^3 and $4.0 \cdot 10^6$ cells/cm^3 for foaming conditions of 10% and 17% of weight reduction, respectively. According to the experimental data, simulation tendencies of cell size and cell density are in similar order of magnitude. A reduction in clamping force and viscosity of the material during injection, and an improvement of the dimensional stability in the final part by foaming, are other features that can also be estimated with the aid of the simulation software.
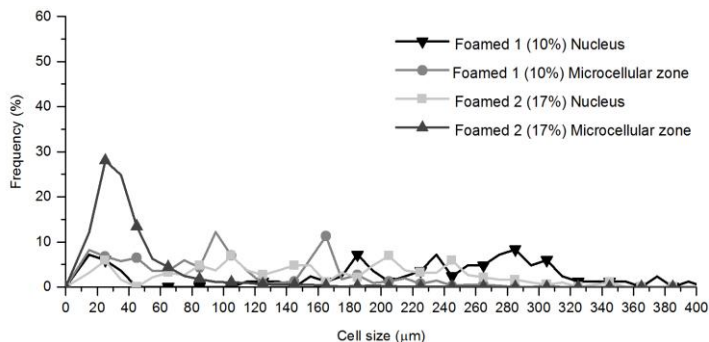
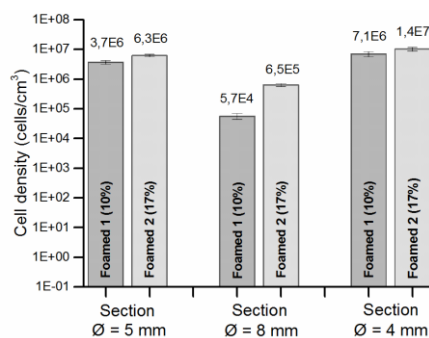Fig. 6. Frequency cell size distribution in Ø = 8 mm section of bar A.

Fig. 7. Cell density in foamed bars.

Mechanical characterization

Fig. 8 (a) shows stress-strain curves corresponding to solid and foamed cylindrical bars. All specimens experimented plastic deformation and necking after the yield point, followed by brittle failure. As the gas content increased, the cellular materials became more brittle [13]. Elastic modulus (Fig. 8 (b)), yield strength (Fig. 8 (c)), yield strain (Fig. 8 (d)) and ultimate strength were taken as tensile properties, due to the large scatter observed in elongation at break. Young's modulus was decreased by 17% and 22% in case of 10% and 17% of weight reduction, respectively, whereas tensile strength was reduced by 18% and 25% according to the two levels of weight reduction. This higher decrease ratio in the yield stress could be due to the negative effect of the bigger voids located in the nucleus on the tensile strength [14]. The same trend has been reported by Lin *et al.* [15]. Regarding specific values, the gap between properties of solid and foamed specimens was strongly reduced, having a specific modulus of 2431, 2192 and 2281 MPa/g·cm^{-3} in solid and foamed samples with 10% and 17% of weight reduction, and a specific tensile strength of 47.3, 42.1 and 42.1 MPa/g·cm^{-3}, respectively. It is noticeable the same level of the yield strain and ultimate strength obtained in all solid and foamed specimens.

Classic theories of conventional foams relate the relative modulus and strength with the relative density by Square-Relationship and Single Blend models [16], respectively. The equations that best fit the experimental data for relative modulus and relative tensile strength are:

$$\frac{E_f}{E_s} = 8.89 \left(\frac{\rho_f}{\rho_s} \right)^2 - 15.02 \left(\frac{\rho_f}{\rho_s} \right) + 7.13 \ \left(R^2 = 0.95 \right) \tag{2}$$

$$\frac{\sigma_f}{\sigma_s} = 7.69\left(\frac{\rho_f}{\rho_s}\right)^2 - 12.66\left(\frac{\rho_f}{\rho_s}\right) + 5.96 \ \left(R^2 = 0.98\right) \tag{3}$$

Where E_f, E_s, σ_f, σ_s, ρ_f and ρ_s are the elastic modulus, tensile strength and apparent density of foamed and solid material. On the other hand, Xu and Kishbaugh [17] developed estimation models of the tensile strength ratio for plane specimens based on the solid skin and foamed area structure. Adapting these equations to a circular section, the calculated yield strength was 39.1 MPa and 32.7 MPa for foamed specimens with 10% and 17% of weight reduction. These values are accurately close to the experimental data, with an associated error of 3% and 5%.

Some works have been carried out relating the mechanical properties to the cell morphology, obtaining an improvement of the elastic modulus and tensile strength with higher cell densities and smaller cell sizes [18, 19]. Nevertheless, in this study, specimens with higher cell densities and smaller cells corresponded to bars injected at the higher level of weight reduction (17%) and, therefore, lower density and mechanical properties were determined. Due to similar thicknesses of the solid skin in all specimens, its effect on the tensile performance could not be determined; although a build-up in the modulus and yield strength as the surface layer gets thicker is expected [20].
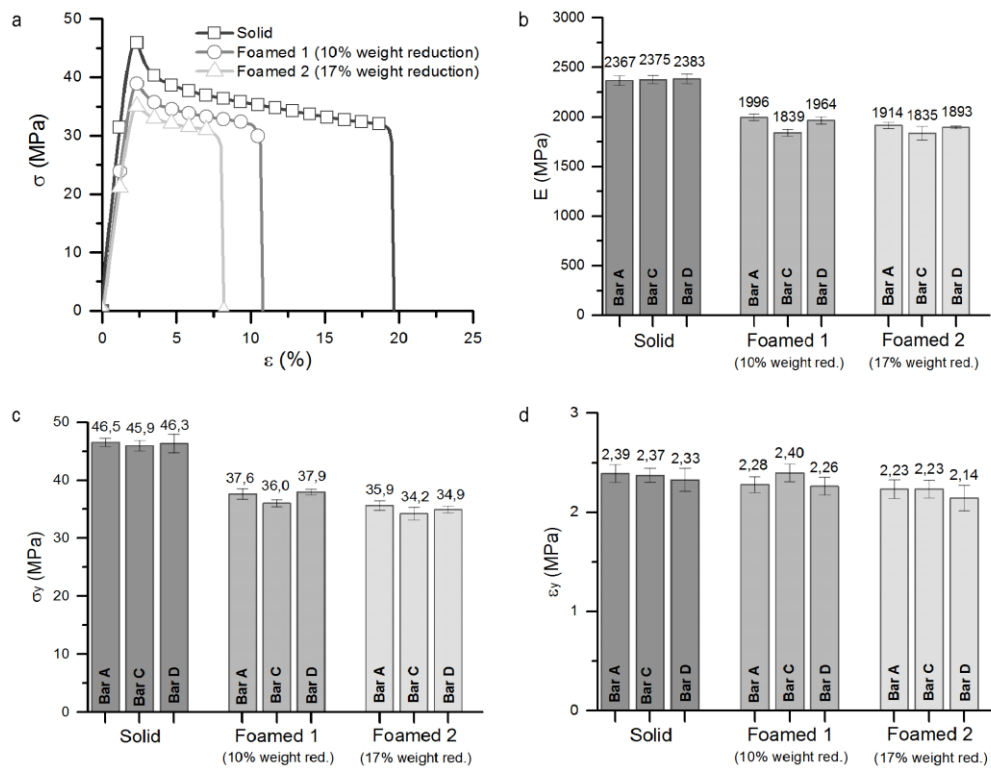

Fig. 8. (a) Tensile stress-strain curves; (b) elastic modulus; (c) yield stress; (d) yield strain obtained in solid and foamed specimens.

Conclusions

In this work, cylindrical bars of 4, 5 and 8 mm in diameter and 300 mm in length were injected at solid and foamed conditions, obtaining two ratios of weight reduction (10% and 17%). A solid skin-foamed core structure was observed. The foamed core was divided into two sections: a nucleus, with bigger cells and irregular cell distribution due to higher expansion rate and bubble coalescence, and a microcellular zone between the nucleus and the skin layer, with more homogenous cell structure. In general, there were no significant differences in morphology

parameters (cell size, cell density, solid skin) between the specimens with two levels of weight reduction. Sections of 4 and 5 mm in diameter presented also similar values of cell size range, cell density and solid skin thickness. Despite the broad range of cell size, most cells were smaller than 40 μm in the microcellular zone, and smaller than 130 μm in the foamed nucleus. Results of cell size and cell density provided by *Moldex 3D®* software showed a similar tendency to the experimental data. Regarding tensile properties, elastic modulus and yield strength decreased with the density. However, yield strain and ultimate strength were almost constant for all solid and foamed specimens. The validity of available models for predicting tensile strength was confirmed, obtaining accurate results. Finally, the evolution of mechanical properties with morphology parameters was analyzed.

Acknowledgements

References

[1] European Environment Agency, Transport sector contribution to total GHG emissions, EEA-32 (2009).
[2] H.C. Kim, T.J. Wallington, Life-Cycle Energy and Greenhouse Gas Emission Benefits of Lightweighting in Automobiles: Review and Harmonization, Environ Sci Technol 47 (2013) 6089-6097.
[3] D. Elduque, I. Claveria, A. Fernandez, C. Javierre, C. Pina, J. Santolaria, Analysis of the Influence of Microcellular Injection Molding on the Environmental Impact of an Industrial Component, Adv Mech Eng doi: 10.1155/2014/793269 (2014).
[4] G.G. Lin, D.J. Lin, L.J. Wang, T.W. Kuo, Absorption and foaming of plastics using carbon dioxide, Res. Chem. Intermed. 40 (2014) 2259-2268.
[5] Y. Dong Hwang, S. Woon Cha, The relationship between gas absorption and the glass transition temperature in a batch microcellular foaming process, Polym. Test. 21 (2002) 269-275.
[6] K. Nadella, V. Kumar, W. Li, Constrained solid-state foaming of microcellular panels, Cell. Polym. 24 (2005) 71-90.
[7] A. Tsuchiya, H. Tateyama, T. Kikuchi, T. Takahashi, K. Koyama, Influence of filler types and contents on foaming structures in ABS microcellular foams, Polym J 39 (2007) 514-523.
[8] G.W. Dong, G.Q. Zhao, Y.J. Guan, G.L. Wang, X.X. Wang, The Cell Forming Process of Microcellular Injection-Molded Parts, J Appl Polym Sci doi: 10.1002/App.40365 (2014).
[9] J.H. Seo, J. Han, K.S. Lee, S.W. Cha, Combined Effects of Chemical and Microcellular Foaming on Foaming Characteristics of PLA (Poly Lactic Acid) in Injection Molding Process, Polym-Plast Technol 51 (2012) 455-460.
[10] A.K. Bledzki, H. Kirschling, M. Rohleder, A. Chate, Correlation between injection moulding processing parameters and mechanical properties of microcellular polycarbonate, J. Cell. Plast. 48 (2012) 301-340.
[11] M.R. Barzegari, D. Rodrigue, The effect of injection molding conditions on the morphology of polymer structural foams, Polym. Eng. Sci. 49 (2009) 949-959.
[12] J. Xu, Microcellular injection molding, Wiley, Hoboken, New Jersey, 2010.
[13] W.T. Kern, W. Kim, A. Argento, E. Lee, D.F. Mielewski, Mechanical behavior of microcellular, natural fiber reinforced composites at various strain rates and temperatures, Polym. Test. 37 (2014) 148-155.
[14] S.C. Chen, J.P. Yang, J.S. Hwang, M.S. Chung, Effects of process conditions on the mechanical properties of microcellular injection molded polycarbonate parts, J. Reinf. Plast. Comp. 27 (2008) 153-165.
[15] C.K. Lin, S.H. Chen, H.Y. Liou, C.C. Tian, Study on Mechanical Properties of ABS Parts in Microcellular Injection Molding Process, ANTEC 2005 Plastics: Annual Technical Conference, Volume 1: Processing, Boston, Massachusetts (USA), 2005, pp. 708-712.
[16] H. Sun, J.E. Mark, Preparation, characterization, and mechanical properties of some microcellular polysulfone foams, J. Appl. Polym. Sci. 86 (2002) 1692-1701.
[17] J. Xu, L. Kishbaugh, Simple modeling of the mechanical properties with part weight reduction for microcellular foam plastic, J Cell Plast 39 (2003) 29-47.
[18] W. Gong, J. Gao, M. Jiang, L. He, J. Yu, J. Zhu, Influence of cell structure parameters on the mechanical properties of microcellular polypropylene materials, J. Appl. Polym. Sci. 122 (2011) 2907-2914.
[19] J.L. Li, Z.L. Chen, X.Z. Wang, T. Liu, Y.F. Zhou, S.K. Luo, Cell Morphology and Mechanical Properties of Microcellular Mucell (R) Injection Molded Polyetherimide and Polyetherimide/Fillers Composite Foams, J Appl Polym Sci 130 (2013) 4171-4181.
[20] S. Wong, J.W.S. Lee, H.E. Naguib, C.B. Park, Effect of Processing Parameters on the Mechanical Properties of Injection Molded Thermoplastic Polyolefin (TPO) Cellular Foams, Macromol. Mater. Eng. 293 (2008) 605-613.